System MgO-SiO$_2$ 2

2.1
Introduction

The two oxides, MgO and SiO$_2$, account for 85 % of the Earth's mantle. Thus, the phase relations in the system MgO-SiO$_2$ (MS), shown in Figs. 2.1 and 2.2, are fundamental for understanding the mineral composition of the mantle. There are five enstatite polymorphs (Mg$_2$Si$_2$O$_6$): protoenstatite, orthoenstatite, low clinoenstatite, high-T clinoenstatite, and high-P clinoenstatite, which can coexist in silica undersaturated compositions with forsterite, wadsleyite, or ringwoodite (Mg$_2$SiO$_4$). At high pressures, high-P clinoenstatite breaks down to majorite at the temperatures above 1,600 °C, and to wadsleyite + stishovite or ringwoodite + stishovite at lower temperatures. Akimotoite and MgSiO$_3$ perovskite appear at progressively still higher pressures. The MgSiO$_3$ perovskite can coexist with periclase (MgO) in the lower mantle.

Univariant phase boundaries in the MS system often serve as end-member reactions for calculating multivariant equilibria in chemically more complex systems. Because of the relatively large number of the univariant boundaries and their importance for the mantle mineralogy, the phase relations in the MS system are often used in experimental studies as a reference temperature-pressure grid for calibration purposes [52]. Due to the lack of absolute calibration points at high temperatures and pressures, such a common reference grid is useful for inter-laboratory comparisons of experimental results.

2.2
Stability of the Enstatite Polymorphs

Orthoenstatite (Pbca) is the only polymorph with a widespread occurrence in the terrestrial rocks, while clinoenstatite (P2$_1$/c) is often found in meteorites (see Reid and Cohen [371], and references therein). The first observation of a multiply twinned terrestrial clinoenstatite was documented by Dallwitz et al. [151]. Subsequent workers have found clinoenstatite-bearing rocks in association with ophiolite complexes (e.g. [275, 391]). Both orthoenstatite and clinoenstatite were first synthesized by Allen et al. [82].

Protoenstatite (Pbcn) was first synthesized by Haraldsen [198]. Proto-enstatite inverts easily to clinoenstatite at the ambient conditions, which led

Atlas [91] to propose that the naturally occurring clinoenstatite is a metastable low-temperature polymorph resulting from the inversion of protoenstatite. However, later phase equilibrium experiments by Sclar et al. [402] and Boyd and England [117] appeared to support the existence of a stable clinoenstatite at low temperatures.

Trommsdorff and Wenk [434] reported an occurrence of untwinned clinoenstatite within kink bands of bronzite crystals. The extreme bending and kinking of bronzite was indicative of the intense deformation experienced by the host gabbro. Orthoenstatite was known to invert to clinoenstatite at temperatures both above and below the experimentally determined boundary when shear stresses were applied [376], and ferrosilite (Fe$_2$Si$_2$O$_6$) also experienced an ortho-rhombic to monoclinic inversion under shearing conditions [297]. This raised the possibility that the occurrences of clinoenstatite in nature were metastable, resulting from the stress-induced inversion of orthoenstatite.

The recognition that nonhydrostatic stresses can affect the location of the orthoenstatite to clinoenstatite boundary, and the discrepancy between the boundaries determined by Sclar et al. [402] and Boyd and England [117] cast some doubt on the true existence of the stability field of clinoenstatite at low temperatures. Grover [187, 188] resolved this issue by reversing the orthoenstatite to clinoenstatite boundary in externally heated cold-seal pressure vessels at 450–750 °C and 0.15–0.4 GPa, thus proving the stability of clinoenstatite (Fig. 2.1).

Perrotta and Stephenson [357] observed that clinoenstatite transformed reversibly to a different monoclinic phase at 995 °C (1 atm), and named the new phase high clinoenstatite. Smith [413] reindexed their X-ray diffraction pattern and suggested that the space group for this phase was C2/c. The P2$_1$/c clinoenstatite stable at low temperatures has since been referred to as low clinoenstatite. The metastable transition from the low to high clinopyroxene was subsequently observed in a variety of compositions on the enstatite-ferrosilite join (e.g. [414, 415, 418]), and the transformation temperatures vary from 995 °C for the pure enstatite to about 300 °C for ferrosilite. High clinoenstatite has the same space group as diopside, which makes it very likely that they both belong to the same solid solution. Solution modeling of the enstatite-diopside joint [19] strongly suggested the existence of a limited field of stability for high clinoenstatite immediately below the melting curve (Fig. 2.3).

The phase relations among the enstatite polymorphs were further complicated by the observation of an orthoenstatite to clinoenstatite transition at high pressures (Fig. 2.4; [23, 259, 466]). This boundary had a much smaller dP/dT slope than the orthoenstatite to low clinoenstatite boundary determined by Sclar et al. [402], Boyd and England [117] and Grover [187, 188]. Experimental data for the orthoferrosilite to clinoferrosilite transition showed a similar discrepancy between the results of Lindsley [293] and Akimoto et al. [79]. Pacalo and Gasparik [23] suggested that this high-pressure (high-P) clinoenstatite was a new phase, very likely a structural analogue of Mg$_2$Ge$_2$O$_6$ clinopyroxene [388]. By analogy, the space group of this high-pressure polymorph was expected to be C2/c, although the phase quenches as P2$_1$/c low clinoenstatite. The structure was also

expected to be different from high clinoenstatite stable at low pressures and high temperatures (high-T clinoenstatite), which crystallizes in the same C2/c space group. This was later confirmed by in-situ X-ray diffraction observations in a diamond cell by Angel et al. [88].

2.3
Protoenstatite to Orthoenstatite Transition and the Stability of High-T Clinoenstatite

The true nature of the protoenstatite to orthoenstatite transition (1) was fully understood only by the solution modeling of the enstatite-diopside join [19]. In a series of papers, Carlson reported new data for the enstatite-diopside join at 1 atm, and presented the evidence for the reappearance of orthoenstatite at 1,370–1,445 °C [130–132, 135]. The data indicated that the Ca contents of the coexisting protopyroxene and pigeonite at 1,295–1,370 °C decrease with increasing temperature (Fig. 2.5). The same trend was observed above 1,370 °C for the coexisting protopyroxene with orthopyroxene and orthopyroxene with pigeonite. This trend indicated that the end-member reactions in the Ca-free system, including the protoenstatite to orthoenstatite transition, were located at higher temperatures than the observed phase relations. This seemingly contradicted the experimentally determined protoenstatite to orthoenstatite transition determined at 985($\pm$10) °C by Atlas [91]. If these observations were correct, they required that the protoenstatite to orthoenstatite boundary appeared at 1 atm at two different temperatures.

The protoenstatite to orthoenstatite boundary was determined at high pressures by Kushiro et al. [290] at 1,200–1,350 °C, and by Anastasiou and Seifert [83] at 1,000–1,300 °C (Fig. 2.3). The results of both studies are consistent with each other and with a straight line passing through 975 °C at 1 atm, in agreement with Atlas [91]. Thus, these data do not indicate that the boundary curves and returns to 1 atm at a higher temperature, as required by the Carlson's [132] data. However, a linear extrapolation of the boundary to higher temperatures was inconsistent with the data of Boyd et al. [119] at the temperatures between 1,550 °C and the solidus. Chen and Presnall [146] attempted to resolve this discrepancy by conducting additional experiments at the temperatures above 1,300 °C. Although, they obtained a reversal at 0.8 GPa and 1,313–1,417 °C consistent with the low-temperature data, the experiments at higher temperatures produced orthoenstatite in violation of a straight protoenstatite to orthoenstatite boundary. In order to satisfy the experimental observations, it was necessary to find such pressure-dependent parameters that would produce an approximately straight boundary in the temperature range 980–1,300 °C and a sharp curve at higher temperatures. A simple ΔV term combined with the ΔH, ΔS, and ΔC_p parameters derived from the Carlson's [132] data at 1 atm by [19] produced a symmetric curve with the pressure maximum at the midpoint between 980 and 1,604 °C. This symmetry was preserved even after introducing additional terms for compressibility or thermal expansion. In contrast, the experimental observations required an asymmetric curve with the pressure maximum around 1,450 °C. This was achieved by introducing a pressure

dependence to the ΔC_p parameter. The solution modeling of the enstatite-diopside join by [19] and updated by [44] gave the parameters for the first three Ca-free end-member reactions listed in Table 2.1. The calculated boundaries and the corresponding experimental data shown in Fig. 2.3 are consistent with the stability of orthoenstatite indicated by the experimental results of Chen and Presnall [146] and even with the data of Boyd et al. [119]. Boyd et al. [119] determined the protoenstatite to orthoenstatite boundary at 1,550 °C. However, the data at higher temperatures apparently apply to the orthoenstatite to high-T clinoenstatite boundary (2); both protoenstatite and high-T clinoenstatite quench as low clinoenstatite and thus are difficult to distinguish in the experimental products.

Carlson's [132] 1-atm data place unusually strong constraints on the enthalpy and entropy parameters of the end-member reactions. Particularly, the parameters for the enstatite end-member reactions are likely to be very close to the true thermodynamic values because the crucial experimental constraints include enstatite-rich compositions. The data make possible a refinement of the corresponding enthalpy differences to a few joules; such precision is currently not possible in the calorimetric measurements. The potential application of the thermochemical data is also hampered by the metastability or limited stability for most of the participating end-member phases, by the uncertainty in the extrapolation of the measurements to high temperatures, and by the small differences in the thermochemical values between the phases in the end-member reactions.

The parameters for the orthoenstatite to high-T clinoenstatite reaction (2) are particularly well constrained by the 1-atm data, and surprisingly close to the values obtained by Lindsley et al. [298]. The enthalpy change in all existing thermodynamic models is consistently lower than the value of 8.4 ± 4.2 kJ/mol estimated by Newton et al. [336] from the enthalpy of solution measurements.

The model volume parameters are in broad agreement with the measured molar volumes. The unit-cell volumes reported by Smith [413] give the volume change for the protoenstatite to orthoenstatite transition of -0.214 J/bar at 1 atm and 25 °C, which compares favorably with the model value of -0.32 J/bar. Nickel and Brey [339] proposed that the difference between the unit-cell volumes of orthoenstatite and clinoenstatite, estimated from the molar volumes of the enstatite-diopside clinopyroxene reported by Newton et al. [336], is in the range of -0.01 to $+0.07$ J/bar, which is consistent with the model value of 0.042 J/bar.

2.4
Orthoenstatite to Low Clinoenstatite Boundary

The study of Grover [187, 188] provides the best constraints on the location of this boundary (4). Grover reversed the boundary in externally heated cold-seal pressure vessels at 450–750 °C and 0.15–0.4 GPa. Molten chloride salts (MgCl$_2$-H$_2$O) were used as a flux to enhance the extremely sluggish transformation rates (1–2 months) and to ensure hydrostatic conditions. The resulting phase boundary can be described by the equation: T (°C) $= 566 + 45P$ (GPa). A linear extrapolation of this boundary to high pressures predicts the stability of low clinoenstatite at higher temperatures

than indicated by the earlier high-pressure studies of Sclar et al. [402] and Boyd and England [117], both conducted in solid-media devices. Shear stresses common in such devices favor the metastable formation of low clinoenstatite from orthoenstatite and thus cannot explain the discrepancy. Yamamoto and Akimoto [466] also reported orthoenstatite forming under presumably hydrostatic conditions at lower temperatures than the linear extrapolation of the Grover's boundary would allow. The experimental observations can only be satisfied if the boundary separating orthoenstatite and low clinoenstatite curves to lower temperatures at high pressures. This is not surprising, considering the small volume change of the transition (-0.003 J/mol, Stephenson et al. [426]); even a small difference in compressibilities could produce a large curvature in the boundary.

Additional constraints were provided by the metastable low to high-T clinoenstatite transition (5), observed at 1 atm and 995 °C [357, 407]. The parameters for the two reactions involving low clinoenstatite and given in Table 2.1 were calculated from the 1-atm temperature of the low to high-T clinoenstatite transition of 995 °C, from the 1-atm temperature of the orthoenstatite to low clinoenstatite transition of 566 °C and the suggested curved extrapolation of the boundary to high pressures, and from the parameters of the orthoenstatite to high-T clinoenstatite transition (2). The resulting volume change of -0.011 J/bar for the orthoenstatite to low clinoenstatite transition (4) is close to the value of -0.003 J/bar measured at 1 atm by Stephenson et al. [426]. The model volume change of -0.053 J/bar for the transition from high-T to low clinoenstatite (5) is close to the value of -0.04 J/bar resulting from the measurements of Smyth ([415], his Fig. 3) on high and low clinohypersthene.

The enthalpy of formation of orthoenstatite from oxides at 970 K of -69.5 kJ/mol (Table 1.1) was obtained by averaging the measurements of Kiseleva et al. [273], Chatillon-Colinet et al. [143] and Brousse et al. [123]. According to Krupka et al. [277, 278], the entropy of orthoenstatite at 970 K is 386.2 J/mol K. The 298 K values for low clinoenstatite from Robie et al. [386] extrapolated to 970 K with the heat-capacity equations of Berman and Brown [97] yield -71.1 kJ/mol for the enthalpy and 383.7 J/mol K for the entropy. Thus, the thermochemical data predict -1.6 kJ/mol for the enthalpy change and -2.5 J/mol K for the entropy change, which is very close to the model values of -1.9 kJ/mol and -2.29 J/mol K, respectively.

2.5
Orthoenstatite to High-P Clinoenstatite Boundary

Yamamoto and Akimoto [466] were the first to report an orthoenstatite to clinoenstatite boundary that was significantly different from the previous determinations at lower pressures (Fig. 2.4). The boundary was determined with a tetrahedral press in hydrothermal synthesis experiments at 625–1,125 °C. The authors pointed out that shear stresses may not had been significant in the presence of water, although, they could had been present at the initial stage of compression and heating, and at the time of quenching. The small dP/dT slope of the boundary determined by Yamamoto and Akimoto [466] was in a sharp contrast with the previous determinations of the orthoenstatite to

clinoenstatite boundary at lower pressures by Sclar et al. [402], Boyd and England [117] and Grover [187, 188], which had very large slopes consistent with the small volume change of the orthoenstatite to low clinoenstatite transition.

Pacalo and Gasparik [23] attempted to resolve this discrepancy by carrying out another study of the orthoenstatite to clinoenstatite transition. The boundary was reversed at 900–1,700 °C and 7–11 GPa. The orthoenstatite to clinoenstatite boundary was also observed by Presnall and Gasparik [24] at 2,140 °C and 11.6 GPa in their study of the melting of enstatite (Fig. 2.6b). The boundary was located in the center of the sample, and separated a single crystal of orthoenstatite in the hot half of the sample from an aggregate of small clinoenstatite crystals in the cold half. A sharp melting curve was present in the hot spot of the sample (2,210 °C) within the orthoenstatite crystal, separating a smooth subsolidus part from the "feathery" part grown during quenching. The triple point for the coexisting orthoenstatite, clinoenstatite and melt was estimated to be at 2,210 °C and 11.8 GPa. These data for the orthoenstatite to clinoenstatite transition can be satisfied with the equation: P (GPa) = 0.0031 T (°C) + 5. The result was consistent with the study by Yamamoto and Akimoto [466]. The obtained dP/dT slope of the orthoenstatite to clinoenstatite boundary was much smaller than indicated by Grover [187, 188] for the orthoenstatite to low clinoenstatite transition. Thus, it was unlikely that the clinoenstatite at both boundaries was the same phase, despite the fact that the quench products were identical. Yamamoto and Akimoto [466] reported orthoenstatite stable at 625 °C, 5.5 GPa. A linear extrapolation of the Grover's boundary would limit the stability of orthoenstatite to much higher temperatures. To satisfy the observations of Yamamoto and Akimoto [466], the orthoenstatite to low clinoenstatite boundary would have to curve to lower temperatures at higher pressures, in the opposite sense than required if the clinoenstatite at the both boundaries were the same phase. Thus, either the Grover's data were incorrect, or the clinoenstatite phase observed at high temperatures and pressures was a different phase, a high-P clinoenstatite.

Another argument against the stability of low clinoenstatite at high pressures and temperatures was the small volume change (−0.003 J/bar) associated with the orthoenstatite to low clinoenstatite transition [426]. If this small volume change was combined with the small slope obtained by Pacalo and Gasparik [23], an entropy change of 0.1 J/mol K would be required. Any small differences between orthoenstatite and clinoenstatite in higher-order properties, such as compressibility, thermal expansion, or heat capacity, would produce a curvature in the boundary. However, the tightly constrained orthoenstatite to high-P clinoenstatite boundary extended over a 1,300 °C temperature interval without any obvious curvature. Thus it was unlikely that the initial assumption of a small volume change for the orthoenstatite to high-P clinoenstatite transition was correct. This was supported by the distinct kink observed on the enstatite melting curve by Presnall and Gasparik [24], which was suggestive of a relatively large volume change for the transition.

The orthopyroxene to clinopyroxene (Pbca-C2/c) transition in the $Mg_2Ge_2O_6$ system has a large volume change of −0.234 J/mol [350, 467]. Germanates are often used as silicate analogues because they experience transitions similar to silicates, but at lower pressures. Ross and Navrotsky [388] analyzed the available data for the $Mg_2Ge_2O_6$ orthopyroxene to clinopyroxene transition; their boundary can be expressed as: $\Delta G = -6{,}880 + 6\,T - 0.234P$.

Thus, the transition in germanate pyroxenes was not a good analogue for the orthoenstatite to low clinoenstatite transition; not only were the clinopyroxene structures different (i.e. low clinoenstatite belongs to the space group P2$_1$/c, whereas the germanate clinopyroxene belongs to C2/c), but also the enthalpy, entropy and volume changes associated with the transition in the germanate system were much larger than the corresponding parameters for the orthoenstatite to low clinoenstatite transition (Table 2.1). However, the transition in the germanate pyroxenes was a very good analogue for the orthoenstatite to high-P clinoenstatite transition. Besides the large volume change, the *dP/dT* slopes were very similar, 26 bar/°C for the germanate vs. 31 bar/°C for the silicate pyroxenes. By analogy, high-P clinoenstatite was expected to crystallize in the space group C2/c.

High-T clinoenstatite also crystallizes in the C2/c space group; however, it must be structurally different from high-P clinoenstatite. High-T clinoenstatite is an end-member in the enstatite-diopside clinopyroxene solution used in the thermodynamic models for calculating the phase relations on the enstatite-diopside join. Experimental data on this join predict the stability of high-T clinoenstatite at higher temperatures and lower pressures than the stability field of orthoenstatite (e.g. [298]). However, the high-P clinoenstatite is stable at lower temperatures and higher pressures than orthoenstatite. In other words, high-T clinoenstatite has a larger entropy and volume than orthoenstatite, while the entropy and volume of high-P clinoenstatite must be smaller. The experimentally observed phase relations on the enstatite-diopside join cannot be reproduced by using the orthoenstatite to high-P clinoenstatite boundary as the end-member reaction [23]. Thus, the high-P clinoenstatite appeared to be a C2/c polymorph different from the high-T clinoenstatite of the C2/c enstatite-diopside solution.

Yamanaka et al. [467] compared the two C2/c structures. The diopside-type-structure, including high-T clinoenstatite, has a highly distorted M2 octahedral site to accommodate the smaller tetrahedral chain with silicon. In $Mg_2Ge_2O_6$ (and isomorphous $Co_2Ge_2O_6$, $Mn_2Ge_2O_6$ and $Fe_2Ge_2O_6$), both octahedra are regular due to the larger size of germanium in the tetrahedral site. The arrangement of the oxygen atoms approximates a cubic closest packing [351]. Apparently, it is the differential compressibility of the octahedral and tetrahedral sites that allows the formation of this structure at high pressures even in silicates.

The volume change and the corresponding enthalpy and entropy changes of the orthoenstatite to high-P clinoenstatite transition (6) were estimated from the phase relations in chemically more complex systems. The parameters listed in Table 2.1 were obtained by the solution modeling of the pyroxene compositions on the enstatite-diopside join [44]. The resulting enthalpy, entropy and volume changes are about 50 % of the values for the analogous transition in the germanate pyroxenes.

2.6
Reactions in the System MgO–SiO₂ at Sublithospheric Pressures

Phase relations in the MS system at very high pressures were reported by Kato and Kumazawa [262], Sawamoto [393], Ito and Takahashi [247, 248], Katsura and Ito [264, 15, 21, 28], and others. The resulting phase relations

based mainly on the experimental observations by [21] are shown in Figs. 2.1 and 2.2.

The forsterite to wadsleyite transition (7) is based on the data of Katsura and Ito [264] at 1,200–1,600 °C and on the observation of the boundary by [24] at 2,240 °C, 16.5 GPa. The parameters (Table 2.1) were derived using ΔH of 30 kJ from the calorimetric measurements of Akaogi et al. [76].

The clinoensleyite to wadsleyite + stishovite boundary (8) was located by [24] at 1,400 °C, 16.5 GPa, with clinoenstatite at higher temperatures, while the clinoenstatite to majorite transition (9) was observed at 2,150 °C, 16.5 GPa, with clinoenstatite at lower temperatures (Fig. 2.6c). This was taken as an evidence for the negative slope of the clinoenstatite to majorite boundary. An experiment at 1,600 °C nominal temperature and 16.6 GPa was very close to the triple point for the coexisting clinoenstatite, majorite, wadsleyite, and stishovite; the boundary between clinoenstatite and wadsleyite + stishovite was located in the cold end of the sample at 1,500 °C, while the portion of the sample located in the hot spot at 1,650 °C transformed completely to majorite. These observations placed the location of the triple point close to 1,600 °C and 16.8 GPa. The parameters given in Table 2.1 for the reactions (8) and (9) are based on these observations and were derived by [44]. The metastable transition from orthoenstatite to majorite (10) can be calculated from (6) and (9), and was used in compositionally more complex systems for calculating the majoritic content of garnet coexisting with aluminous orthopyroxene.

The parameters for reactions (8) and (9) predict a close-to-infinite slope of the majorite to wadsleyite + stishovite transition (11), which is supported by experimental observations [21]. The boundary was located in the center of a sample at 1,600 °C, 17.5 GPa, which is at the same temperature as the triple point for the coexisting enstatite, majorite, wadsleyite, and stishovite at 16.8 GPa. These observations suggested a small volume change for reaction (11).

A strong reaction to akimotoite was observed at 1,600 °C and 17.8 GPa [21]. At 1,500 °C and 18.2 GPa, only a few crystals of wadsleyite were present in the cold end of the sample, made mostly of akimotoite, because of the compositional inhomogeneities in the starting material. These observations indicated that akimotoite is stable at lower pressures than reported earlier by Sawamoto [393]. The triple point for the coexisting wadsleyite, stishovite, majorite, and akimotoite was thus located at 1,600 °C and 17.5–17.8 GPa. Its position precludes a large positive dP/dT slope for the wadsleyite + stishovite to akimotoite transition (12), indicated by the phase diagrams of Kato and Kumazawa [262] and Sawamoto [393], but is more consistent with a negative slope predicted by Ito and Navrotsky [246]. A large positive slope of the wadsleyite + stishovite to akimotoite transition would limit the stability field of the assemblage ringwoodite + stishovite to very low temperatures. In contrast, most experimental studies predict the high-temperature stability limit of the ringwoodite + stishovite assemblage to be in the range from 1,250 [246] to 1,600 °C [393]. The parameters for reaction (12) given in Table 2.1 are the same as derived by [21] on the basis of these observations.

The wadsleyite to ringwoodite transition (13) is one of the more often studied phase boundaries. The width of the wadsleyite + stishovite stability field at 1,000 °C is about 1 GPa [77, 257], which places the transition at 17 GPa.

At 1,600 °C, Katsura and Ito [264] located the transition at 20.8 GPa. The lack of ringwoodite in an experiment by [21] at 2,000 °C nominal temperature and 22.4 GPa (1,850 °C in the cold end of the sample) indicated a slightly larger slope than proposed by Katsura and Ito [264], as shown by the parameters for (13) in Table 2.1, taken from [21].

The ringwoodite + stishovite to akimotoite transition (14) is usually placed at 1,000 °C at 19–19.5 GPa [246, 257]. Ito and Navrotsky [246] showed that the boundary has a negative slope, which is consistent with the majority of the experimental observations. The parameters calculated from (12) and (13) predict the transition at 1,000 °C at 19.5 GPa (Table 2.1).

The parameters for the majorite to akimotoite transition (15) can be calculated from (11) and (12). This phase boundary was observed in an experiment at 2,030 °C and 21.9 GPa, which suggested the presence of a strong curvature in the boundary. Such a curvature could be caused by a disorder in majorite with increasing temperature, as proposed by Hatch and Ghose [208], McMillan et al. [320], and [35]. In view of the evidence for the disorder in the end-member majorite, Gasparik [28] proposed that this disorder was the dominant cause for the observed curvature in the majorite to akimotoite boundary, and included an excess heat capacity term in the majorite-forming reactions to produce the curvature (Table 2.1).

Ito and Takahashi [248] determined the positions of two perovskite-forming transitions: akimotoite to perovskite (16) and ringwoodite to perovskite + periclase (17). The corresponding parameters listed in Table 2.1 were taken from [44].

The breakdown of majorite to perovskite (18) was observed at 2,400 °C and 22.4 GPa by [21]. Majorite was located in the sample at higher temperatures, which is consistent with the positive slope of the reaction, and in agreement with Sawamoto [393]. The assemblage perovskite + periclase was synthesized at 2,000 °C and 22.6 GPa, and was close to stability at 2,450 °C, which is consistent with the zero slope of the reaction (19) corresponding to the breakdown of wadsleyite to perovskite and periclase. The breakdown of wadsleyite to majorite and periclase (20), predicted to occur close to the solidus in Fig. 2.2, and the metastable breakdown of ringwoodite to majorite and periclase (21) can be calculated from the parameters already derived.

Finally, the parameters for the metastable reaction of stishovite + Mg$_2$SiO$_4$ with the calcium ferrite structure to majorite (22) will be derived later by modeling the mixing properties of the NaAlSiO$_4$–Mg$_2$SiO$_4$ solid solution.

2.7
Melting Relations in the System MgO–SiO$_2$

Bowen and Andersen [112] studied the MS system at 1 atm and showed that enstatite melted incongruently to liquid and forsterite (Fig. 2.6a). Davis and England [156] determined the melting curve of forsterite to 5 GPa. Boyd et al. [119] studied the melting behavior of enstatite to 4.7 GPa. Chen and Presnall [146] documented the shift of the eutectic between forsterite and enstatite with increasing pressure and estimated the pressure of the singular point at which

enstatite begins to melt congruently to be at 0.13 GPa. Ohtani and Kumazawa [344] and Presnall and Walter [365] extended the melting curve of forsterite to 16.5 GPa. The melting curve of enstatite was determined by Kato and Kumazawa [262, 263] and Presnall and Gasparik [24]. Gasparik [21] extended the melting relations to the stability field of MgSiO$_3$ perovskite at 22.6 GPa.

Presnall and Gasparik [24] reinvestigated the melting curve of enstatite because the previous determination by Kato and Kumazawa [262, 263] at 3, 7, and 20 GPa indicated a significant increase in the *dP/dT* slope of the enstatite melting curve between 7 and 20 GPa; the slope was inconsistent with the extrapolation of the low-pressure data beyond 7 GPa using the Simon equation. The melting curve was constrained with six experiments at 10–16.5 GPa. Two invariant points were located, one for orthoenstatite, clinoenstatite, and melt at 2,230 °C, 11.9 GPa, and the other for clinoenstatite, majorite and melt at 2,340 °C, 16.4 GPa. The melting temperatures were up to 160 °C higher than those of Kato and Kumazawa [262, 263]. The melting curve of orthoenstatite can be expressed with the following Simon equation: P (GPa) = 1.9 {[T (K)/1,840]$^{6.6}$–1}.

Presnall and Gasparik [24] also carried out four experiments on the enstatite-forsterite join at 16.5 GPa. The pure MgSiO$_3$ composition produced coexisting majorite and melt at 2,350 °C. Pure forsterite melted incongruently at 2,380 °C to anhydrous phase B, Mg$_{14}$Si$_5$O$_{24}$, in addition to melt and periclase. Single crystals from this experiment were used for the structure determination by Finger et al. [17]. The third experiment with the starting composition En$_{80}$Fo$_{20}$ (wt %) showed the eutectic melting at 2,250 °C. Microprobe analyses of the quench crystals yielded compositions ranging from 51.0 to 74.7 wt % enstatite, with the average at 66.6 wt % enstatite. The fourth experiment with the En$_{40}$Fo$_{60}$ composition showed the eutectic melting at 2,240 °C, with a narrow rim of forsterite/wadsleyite separating the subsolidus forsterite/wadsleyite + majorite assemblage from the quenched melt region. Therefore, the eutectic melt composition was more enstatite rich than the starting bulk composition. The forsterite to wadsleyite boundary separated an irregular layer of forsterite in the hot spot from wadsleyite + majorite located on both sides of the forsterite layer. The boundary was consistent with a linear extrapolation of the forsterite to wadsleyite transition determined by Katsura and Ito [264] in the temperature range 1,200–1,600 °C. The majorite + wadsleyite to clinoenstatite + wadsleyite boundary was located in the cold end of the sample at 2,150 °C. The average of the microprobe analyses from the quenched melt region was 64.7 wt % enstatite, which was very close to the average quenched melt composition from the experiment with the En$_{80}$Fo$_{20}$ composition. Because the two starting compositions were on the opposite sides of the eutectic, the near coincidence of the two melt compositions indicated that they both represented very closely the eutectic composition.

Gasparik [21] extended the melting relations on the enstatite-forsterite join to the stability field of MgSiO$_3$ perovskite by determining the eutectic melting temperatures and compositions in two experiments at 22.4 and 22.6 GPa (Fig. 2.6d). The experiment at 22.4 GPa produced the eutectic melting of the bulk composition En$_{40}$Fo$_{60}$ (wt %) in the hot spot of the sample at 2,430 °C. The melt, present as quenched crystals, was in contact with both majorite and wadsleyite. The average composition of the quenched melt was close to 60 wt % enstatite. Most of the sample consisted of

perovskite + wadsleyite; the boundary between perovskite and majorite was close to the hot spot at 2,400 °C. The boundary was marked by a single row of periclase crystals completely enclosed in a continuous layer of wadsleyite. Thus, perovskite was nowhere in contact with periclase, majorite, or quenched melt. The experiment at 22.6 GPa produced the eutectic melting of the bulk composition En$_{60}$Fo$_{40}$ (wt %) in the center of the sample at 2,450 °C. The subsolidus part of the sample consisted of the assemblage perovskite + wadsleyite, both of which were in contact with the quenched melt. The large area of the quenched crystals allowed broad-beam analyses, which were taken only from the parts showing fine quench texture. The average melt composition was En$_{56}$Fo$_{44}$ (wt %), with a relatively small spread between 50 and 60 wt % enstatite. The results indicated that the invariant point for the coexisting majorite, perovskite, wadsleyite, and liquid was located close to 2,430 °C and 22.4 GPa.

A comparison of the eutectic melt compositions at 22.4–22.6 GPa with the compositions reported by Presnall and Gasparik [24] at 16.5 GPa indicates that the forsterite content of the eutectic melt in equilibrium with majorite and wadsleyite keeps increasing with pressure. Since it is likely that the temperature difference between the eutectic temperature and the melting temperature of majorite is somewhat larger at 22.4–22.6 GPa than 100–130 °C found by Presnall and Gasparik [24] at 16.5 GPa, the melting temperature of MgSiO$_3$ perovskite at the triple point for the coexisting majorite, perovskite, and melt (22.5 GPa) should be close to 2,600 °C [21].

The experiments at low pressures (e.g. [146]), and particularly the qualitative observation that the incongruent melting of enstatite at 1 atm is replaced with the congruent melting at higher pressures, indicate that the eutectic composition on the enstatite-forsterite join becomes more forsteritic with increasing pressure. On the basis of this trend, Takahashi [428], Herzberg et al. [220], and Herzberg and Ohtani [218] estimated the position of the enstatite-forsterite eutectic. Herzberg and O'Hara [217] had also proposed a phase diagram indicating their preferred location for the forsterite-majorite eutectic at 15 GPa, although no constraining experimental data at 15 GPa existed at that time. All these estimates indicated eutectic compositions much more enriched in forsterite than the compositions determined by Kato and Kumazawa [263], Gasparik [21], Presnall and Gasparik [24], and more recently by Herzberg and Zhang [219] and Presnall et al. [366]. These experimental results showed that the rate of migration of the enstatite-forsterite eutectic toward forsterite with increasing pressure slows down. Thus the compositions of the eutectic, if based only on the experimental observations in the simple system MgO-SiO$_2$, appear to be inconsistent with the formation of the upper mantle by a eutectic-like partial melting [24].

2.8
Stability of the SiO$_2$ Polymorphs

Figure 2.7 shows the stability of six SiO$_2$ polymorphs: low quartz, high quartz, tridymite, cristoballite, coesite and stishovite. The low to high quartz transition determined by Cohen and Klement [148] is minor, and therefore was omitted

in the calculation of the phase diagrams in this book. The quartz to coesite boundary (23) shown in the figures corresponds to the slightly curved boundary of Bohlen and Boettcher [107], although this transition was approximated as linear in the calculations with the parameters given in Table 2.1 [37]. There was no intention while deriving these parameters to obtain the properties of coesite that would satisfy the coesite to stishovite boundary of Zhang et al. [36].
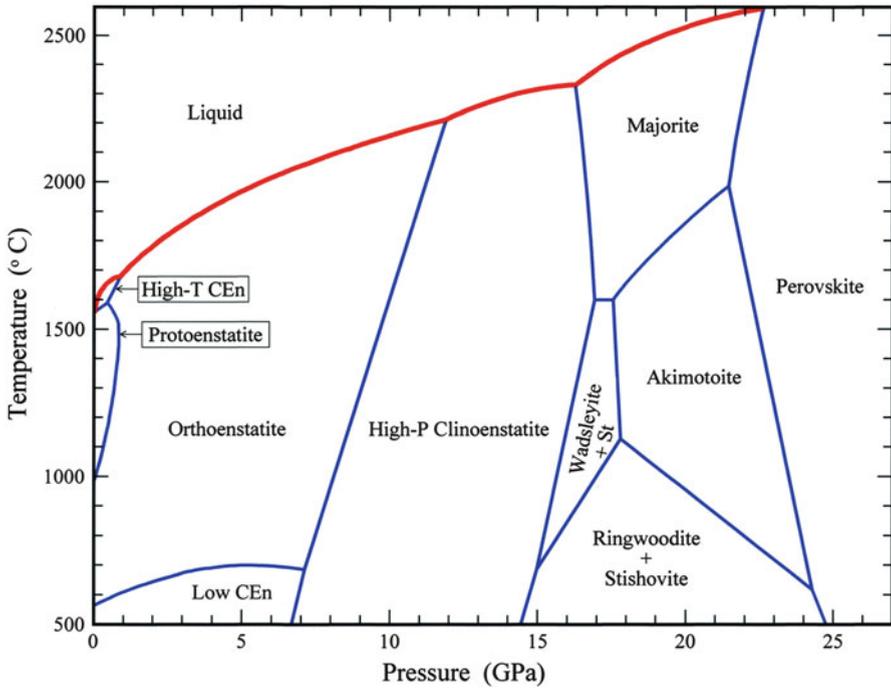

Fig. 2.1. Temperature-pressure phase diagram for the $MgSiO_3$ system calculated using the parameters in Table 2.1. The melting curve is after Boyd et al. [119], [21] and [24]
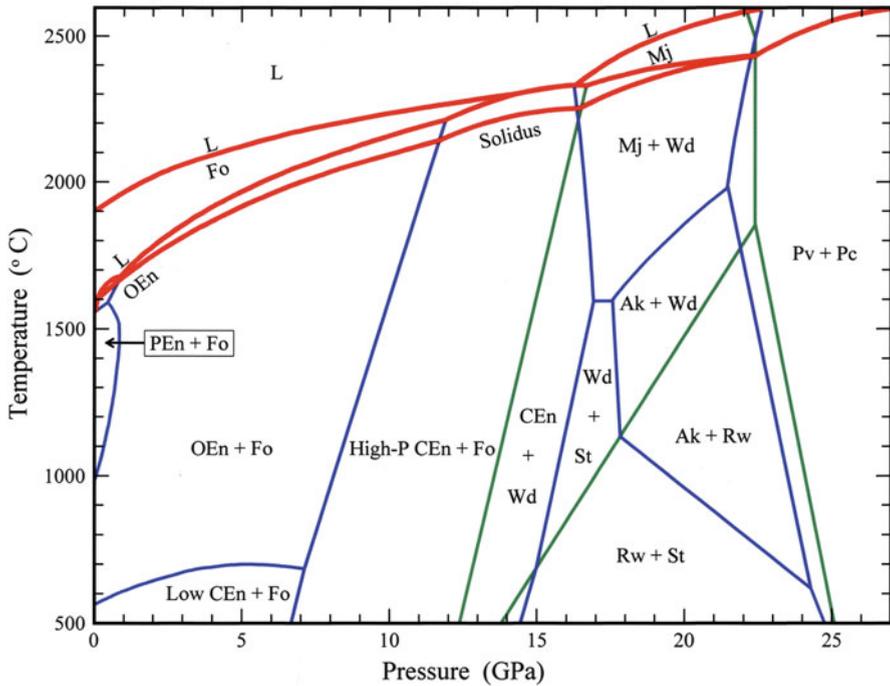
Fig. 2.2. Temperature-pressure phase diagram for the join $MgSiO_3$–Mg_2SiO_4 calculated using the parameters in Table 2.1. The solidus is based on Chen and Presnall [146], [21] and [24]. The melting curve of forsterite is after Davis and England [156] and Presnall and Walter [365]
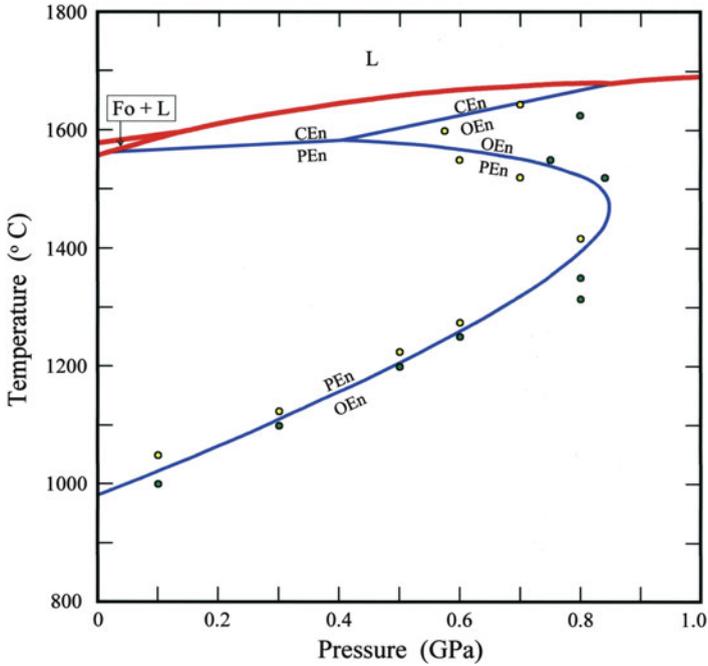
Fig. 2.3. Temperature-pressure phase diagram for the MgSiO₃ system at pressures below 1 GPa, showing the calculated univariant phase boundaries (1–3) and the corresponding experimental data indicating the stability of protoenstatite or high-T clinoenstatite (*yellow*) and ortho-enstatite (*green*) by Boyd et al. [119], Anastasiou and Seifert [83], and Chen and Presnall [146]
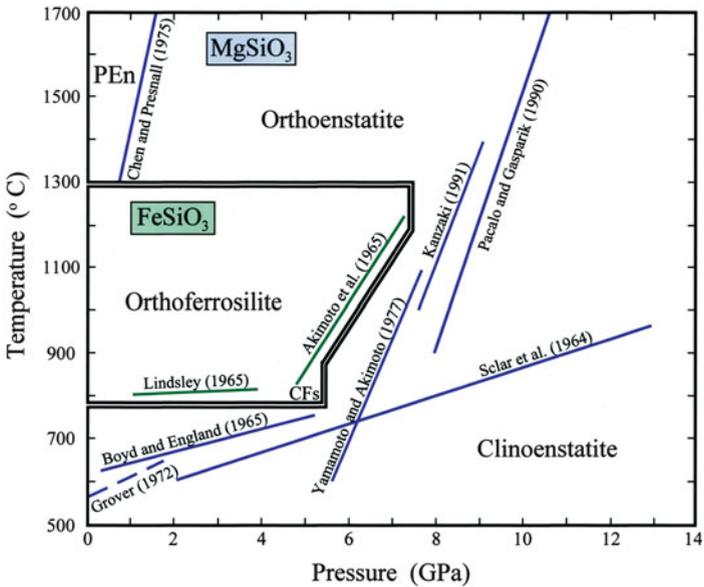

Fig. 2.4. A summary of the experimental observations concerning the orthopyroxene to clinopyroxene transitions in the end-member systems MgSiO₃ and FeSiO₃ (After [23])
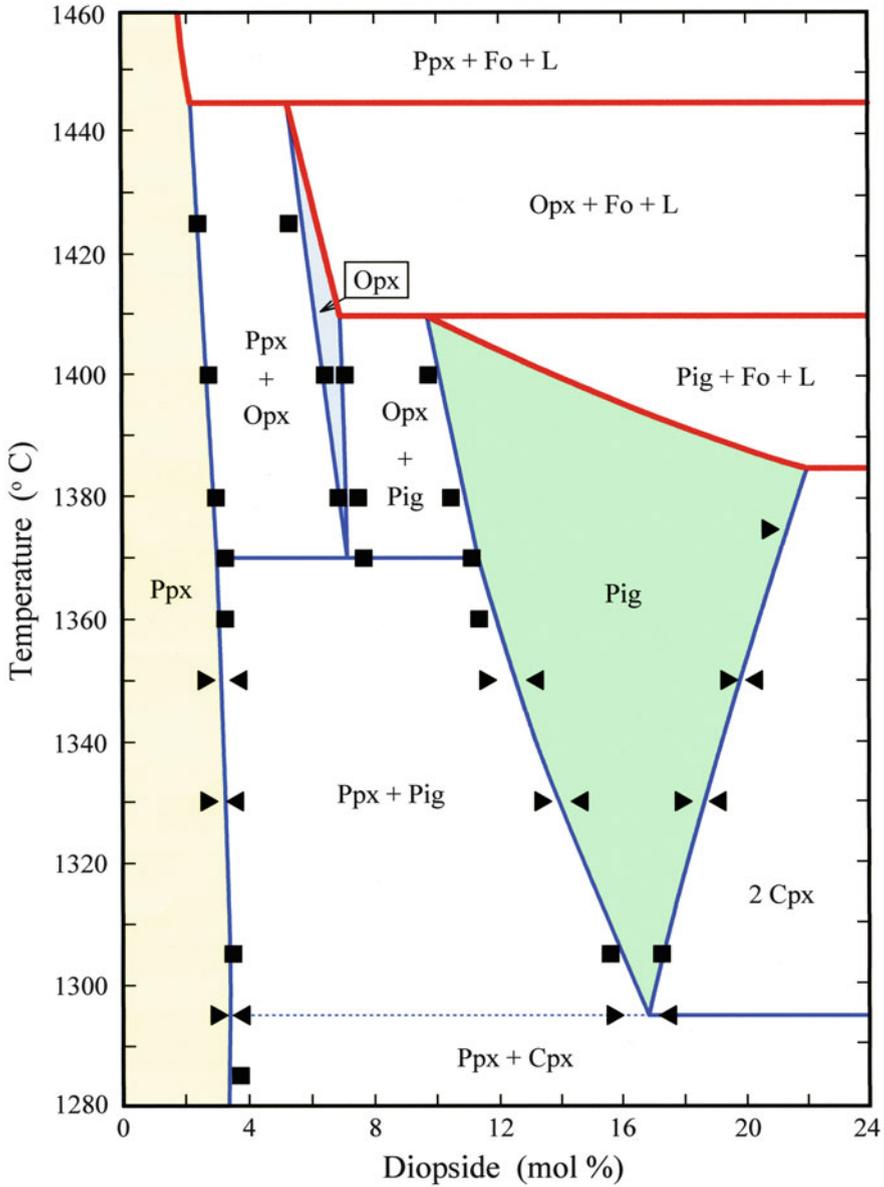
Fig. 2.5. Calculated temperature-composition phase diagram for the enstatite-rich portion of the enstatite-diopside join at 1 atm, and the experimental data of Carlson [132]. *Triangles* indicate reversals, *squares* correspond to synthesis experiments. *Heavy lines* indicate melting relations
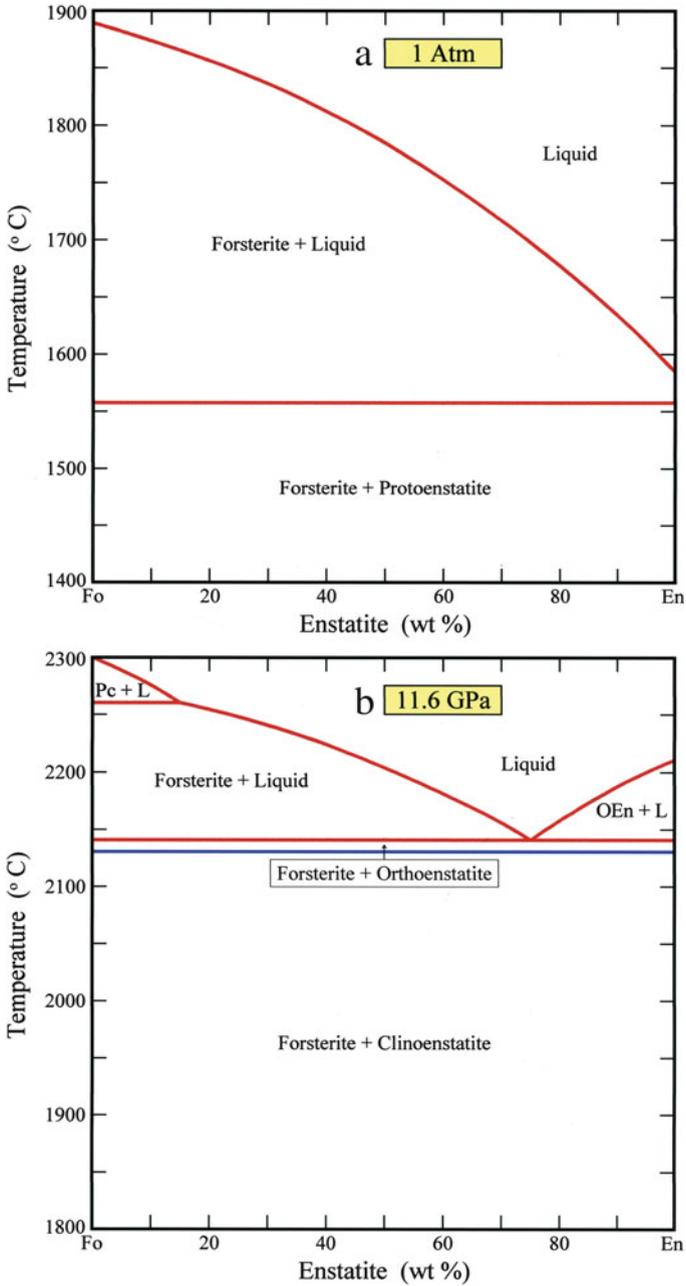
Fig. 2.6. Temperature-composition phase diagrams for the system forsterite-enstatite (wt %). *Rectangles* show the range of the observed compositions of the quenched melt by [21] and [24], with *dots* indicating average values. The phase relations at 1 atm (**a**) are by Bowen and Andersen [112], at 11.6 (**b**) and 16.5 GPa (**c**) by [24], and at 22.5 GPa (**d**) by [21]
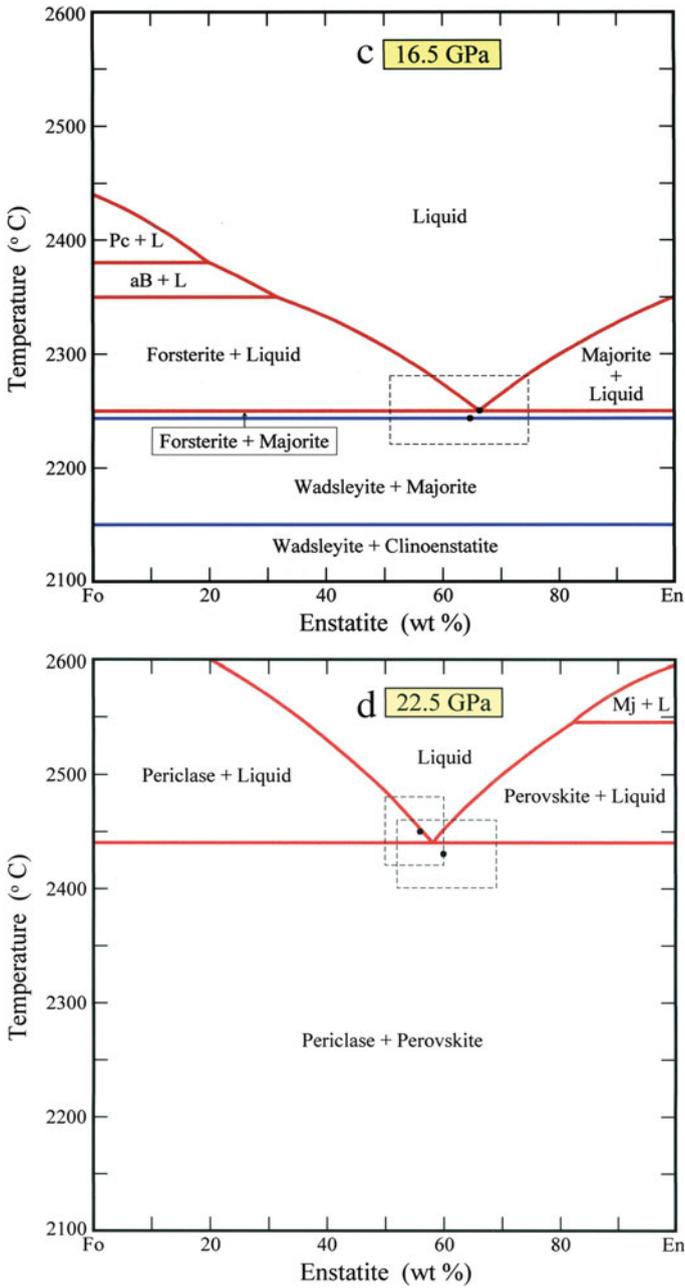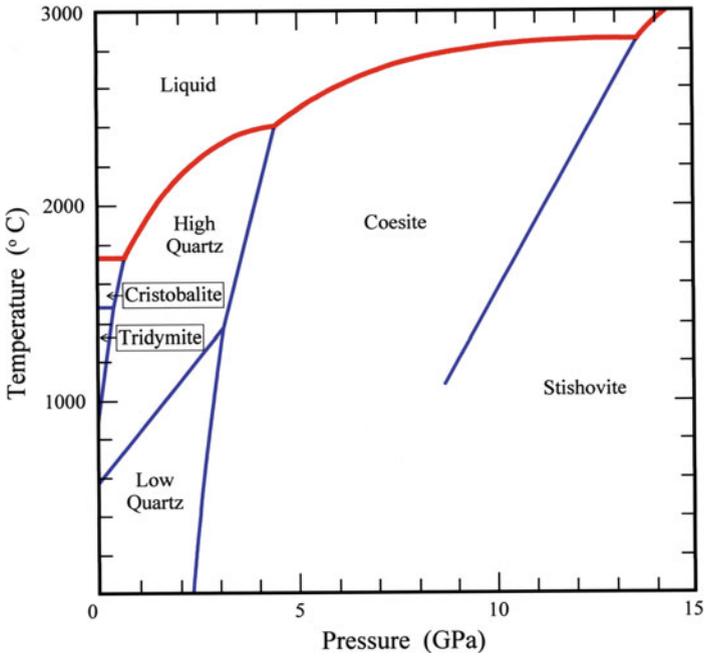
Fig. 2.6. (continued)

Fig. 2.7. Temperature-pressure phase diagram for SiO_2. Subsolidus boundaries are from Tuttle and Bowen [436], Cohen and Klement [148], Mirwald and Massonne [323], Bohlen and Boettcher [107] and [36]. Melting is after Jackson [249], Kanzaki [258] and [36]

Table 2.1. Equilibria in the system MgO-SiO$_2$ and the corresponding parameters

#	Equilibrium	$\Delta G_{T,P} = \Delta H_T^\circ - T\Delta S_T^\circ - cT^{1.2} + P\Delta V_T^\circ - bP^2$
1	PEn = OEn	$\Delta G(1) = -17{,}932 + 35.55T - 0.6T^{1.5}(1-633 \times 10^{-8}P) - 0.32P$
2	OEn = hEn	$\Delta G(2) = 3{,}457 - 1.95T + 0.042P - 10^{-7}P^2$
3	PEn = hEn	$\Delta G(3) = \Delta G(1) + \Delta G(2) = -14{,}475 + 33.6T - 0.6\,T^{1.5}$ $(1 - 633 \times 10^{-8}P) - 0.278P - 10^{-7}P^2$
4	OEn = lEn	$\Delta G(4) = -1{,}921 + 2.29T - 0.011P + 10^{-7}P^2$
5	hEn = lEn	$\Delta G(5) = \Delta G(4) - \Delta G(2) = -5{,}378 + 4.24T - 0.053P + 2 \times 10^{-7}P^2$
6	OEn = CEn	$\Delta G(6) = 3{,}300 + 2.5T - 0.08P$
7	Fo = Wd	$\Delta G(7) = 30{,}000 + 6.7T - 0.284P$
8	CEn = Wd + St	$\Delta G(8) = 77{,}500 + 12.8T - 0.6P$
9	2CEn = MgMj	$\Delta G(9) = 135{,}900 + 157.6T - 30T^{1.2} - 0.88P - 10^{-6}P^2$
10	2OEn = MgMj	$\Delta G(10) = \Delta G(9) + 2\Delta G(6) = 142{,}500 + 162.6T - 30T^{1.2} - 1.04P - 10^{-6}P^2$
11	MgMj = 2Wd + 2St	$\Delta G(11) = 19{,}100 - 132T + 30T^{1.2} - 0.32P + 10^{-6}P^2$
12	Wd + St = 2Ak	$\Delta G(12) = 35{,}550 - 1.2T - 0.19P$
13	Wd = Rw	$\Delta G(13) = 10{,}700 + 7.6T - 0.12P$
14	Rw + St = 2Ak	$\Delta G(14) = \Delta G(12) - \Delta G(13) = 24{,}850 - 8.8T - 0.07P$
15	MgMj = 4Ak	$\Delta G(15) = \Delta G(11) + 2\Delta G(12) = 90{,}200 - 134.4T + 30T^{1.2} - 0.7P + 10^{-6}P^2$
16	Ak = MgPv	$\Delta G(16) = 55{,}000 - 4.4T - 0.21P$
17	Rw = MgPv + Pc	$\Delta G(17) = 101{,}325 - 7.6T - 0.38P$
18	MgMj = 4MgPv	$\Delta G(18) = \Delta G(15) + 4\Delta G(16) = 310{,}200 - 152T + 30T^{1.2} - 1.54P + 10^{-6}P^2$
19	Wd = MgPv + Pc	$\Delta G(19) = \Delta G(17) + \Delta G(13) = 112{,}025 - 0.5P$
20	4Wd = MgMj + 4Pc	$\Delta G(20) = 4\Delta G(19) - \Delta G(18) = 137{,}900 + 152T - 30T^{1.2} - 0.46P - 10^{-6}P^2$
21	4Rw = MgMj + 4Pc	$\Delta G(21) = 4\Delta G(13) + \Delta G(20) = 180{,}700 + 182.4T - 30T^{1.2} - 0.94P - 10^{-6}P^2$
22	2MS + 2St = MgMj	$\Delta G(22) = -37{,}000 + 143.4T - 30T^{1.2} - 0.268P - 10^{-6}P^2$
23	Q = Cs	$\Delta G(23) = 4{,}000 + 2T - 0.22P$
24	Fo + Q = OEn	$\Delta G(24) = -4{,}600 + T - 0.36P$

Phase Diagrams for Geoscientists
An Atlas of the Earth's Interior
Gasparik, T.
2014, XI, 462 p. 113 illus., 112 illus. in color., Hardcover
ISBN: 978-1-4614-5775-6